

SOFT INTERACTIONS

RALPH ENGEL

*Bartol Research Institute, University of Delaware
217 Sharp Lab, Newark DE 19716, USA
E-mail: eng@lepton.bartol.udel.edu*

A brief introduction to the theory and phenomenology of soft interactions is given, focusing on total and elastic cross sections and multiparticle production.

1 Introduction

The description of soft hadronic multiparticle production within QCD is one of the long-standing, unsolved problems. In recent years progress has been made in understanding soft QCD processes in lattice calculations¹ and also the modified leading-log approximation proved to be a remarkable powerful tool². In this article we focus on another method which is the investigation of predictions implied by unitarity and analyticity of scattering amplitudes and general features of gauge field theories. We will discuss basic concepts and predictions of general nature rather than one or several models in detail, emphasizing a pedagogical presentation of the underlying ideas. The aim is to supply the reader with a basic theoretical framework to understand the more specific contributions to this conference. More detailed discussions of soft interactions and related topics can be found in other reviews^{3,4,5,6,7,8}.

2 Regge amplitude

Cross sections and amplitudes at low energy are fairly well understood in terms of production and decay of a single or a few resonances, as shown in Fig. 1a. With increasing collision energy more and more resonances (with increasing mass and decay width) contribute to the total cross section. This seems to render any approach, which is based on summing all resonance contributions to extrapolate to high energy, infeasible. However, under certain conditions this summation can be carried out and the Reggeon amplitude is obtained⁹.

Because of angular momentum conservation it is convenient to expand the scattering amplitude $A(s, t)$ in terms of partial waves $a_l(s)$ for fixed angular

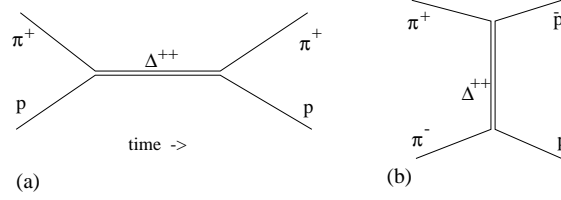


Figure 1. Production and decay of Δ^{++} in the s -channel (a), and a interaction obtained by crossing with Δ^{++} in the t -channel (b).

momentum l

$$A(s, t) = 16\pi \sum_{l=0}^{\infty} (2l+1) a_l(s) P_l(\cos \theta), \quad (1)$$

with θ being the scattering angle in c.m. frame and P_l the Legendre functions of the first kind^a. For resonance exchange the amplitude is of the well known Breit-Wigner form $a_l \sim 1/(s - m_l^2 + im_l\Gamma_l)$.

One of the important assumptions in Regge theory is that of maximum analyticity of the scattering amplitude, which holds in gauge field theories. The amplitude is an analytic function and has only physics-implied singularities. Thus, if the amplitude is completely known for a given scattering process, then the amplitudes for all other channels, which are related to the former one by crossing, can be obtained by analytic continuation of this amplitude. An example for this is given in Fig. 1b. After crossing from the s -channel to the t -channel Eq. (1) reads

$$A(s, t) = 16\pi \sum_l (2l+1) a_l(t) P_l(z_t), \quad z_t = \cos \theta_t = \frac{2s}{t - s_0} + 1. \quad (2)$$

The scale s_0 is related to the masses of the particles ($s_0 \sim 1\text{GeV}^2$). The partial wave amplitude describes now the exchange of a particle with angular momentum l in the t -channel $a_l(t) \sim 1/(t - m_l^2 + im_l\Gamma_l)$.

Using Cauchy's theorem the sum (2) is re-written as integral (Sommerfeld-Watson transformation)

$$A(s, t) = \sum_{\tau=\pm 1} \frac{16\pi}{2i} \int_{C_1} dl (2l+1) \left(\frac{1 + \tau e^{-i\pi l}}{\sin(\pi l)} \right) a_l(t) P_l(-z_t), \quad \tau = \pm 1, \quad (3)$$

^aFor sake of clarity we omit here all spin-related complications.

where the signature $\tau = \pm 1$ separates the sum into even and odd integer angular momenta. The splitting of the partial sum into positive and negative signature contributions is needed to ensure convergence of the integral. The integration contour runs along both sides of the positive $\Re\{l\}$ axis in the complex l plane (see Fig. 2a).

In (3) the partial wave amplitude has to be extended to continuous values of l . This is done by employing the experimentally established, approximate relation between resonance mass and total angular momentum $m_l^2 = al + m_0^2$ with a and m_0 being constants specific to the group of resonances. Fig. 2 shows an example for meson resonances. From the structure of the partial wave amplitude

$$a_l \sim \frac{1}{t^2 - m_l^2} = \frac{1}{t - m_0^2 - al} \sim \frac{1}{l - t/a + m_0^2/a} = \frac{1}{l - \alpha(t)} \quad (4)$$

follows that there is a singularity for $l = \alpha(t)$ with $\alpha(t) = (t - m_0^2)/a$. The function $\alpha(t)$, called Regge trajectory, is in general a nonlinear complex function of t and related to the quantum numbers of the hadrons whose mass-angular momentum relation it describes.

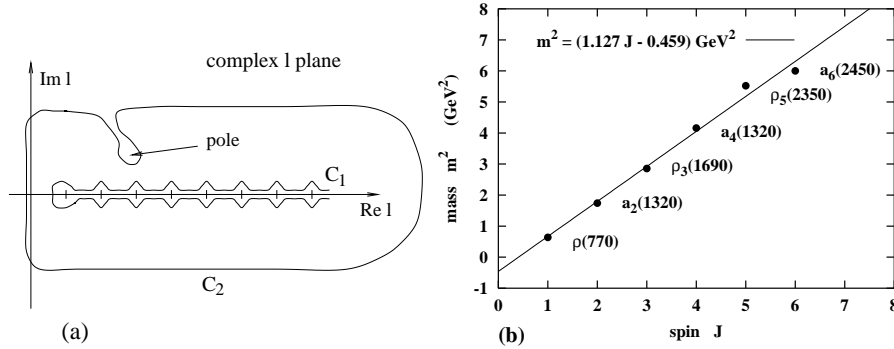


Figure 2. (a) Integration contours for Sommerfeld-Watson transform, and (b) mass-spin relation for ρ and s mesons (Chew-Frautschi plot).

Assuming that $l = \alpha(t)$ is the only singularity due to $a_l(t)$ we can displace the integration contour in Fig. 2a from C_1 to C_2 . The behaviour of the integrand leads to a vanishing contribution from the semi-circle at infinity. Neglecting the contribution from $\Im m\{l\} = -1/2$ all that is left is the contribution of the pole at $l = \alpha(t)$. Thus the final amplitude can be written

as

$$A(s, t) = -\frac{1 + \tau e^{-i\pi\alpha(t)}}{\sin(\pi\alpha(t))} \beta(t) P_{\alpha(t)}(-z_t) , \quad (5)$$

with $\beta(t)$ standing for the residue and other unimportant factors.

Finally, the Regge amplitude is obtained by going to the high-energy limit $s \gg s_0$

$$P_{\alpha_k(t)} \left(-\frac{2s}{t-s_0} - 1 \right) \xrightarrow{s \rightarrow \infty} \left(\frac{s}{s_0} \right)^{\alpha_k(t)} \quad (6)$$

and reads

$$A(s, t) = \sum_k \eta(\alpha_k(t)) \beta_k(t) \left(\frac{s}{s_0} \right)^{\alpha_k(t)} . \quad (7)$$

The index k represents the sum over all contributing Regge trajectories and η is the signature factor of the Regge trajectory k

$$\eta(\alpha_k(t)) = -\frac{1 + \tau e^{-i\pi\alpha_k(t)}}{\sin(\pi\alpha_k(t))} . \quad (8)$$

A single term in the sum (7) describes the contribution of an infinite number of particles exchanged in the t -channel. Each of these groups of particles is represented in the amplitude by a quasi-particle, called reggeon, with the same quantum numbers.

3 Cross section phenomenology

3.1 Regge-based fits

Knowing the Regge trajectories from the measured masses of mesons and baryons, Eq. (7) can be used to predict the energy-dependence of elastic and total cross sections

$$\frac{d\sigma_{\text{ela}}}{dt} = \frac{1}{16\pi s^2} |A(s, t)|^2 , \quad \sigma_{\text{tot}} = \frac{1}{s} \Im m(A(s, t=0)) . \quad (9)$$

The last relation employs the optical theorem and follows from unitarity^b. Using furthermore the parametrization $\beta^2(t) = g^2 \exp\{B_0 t\}$ and considering

^bThe masses of the scattering particles are neglected.

only the highest Regge trajectory, one gets with $\Delta = \alpha(0) - 1$

$$\begin{aligned}\sigma_{\text{ela}} &= (1 + \rho^2) \frac{g^2}{16\pi} \left(\frac{s}{s_0} \right)^{2\Delta} \exp \{ B_{\text{ela}} t \}, & \rho &= \frac{\Re A(s, t)}{\Im A(s, t)} \Big|_{t=0} \\ \sigma_{\text{tot}} &= g \left(\frac{s}{s_0} \right)^\Delta, & B_{\text{ela}} &= B_0 + 2\alpha'(0) \ln s\end{aligned}\quad (10)$$

There are several shortcomings of the amplitude (7). The total cross section is predicted to have the energy dependence $\sigma_{\text{tot}} \sim s^\Delta$. The intercept of the highest known Regge trajectory is about $\alpha(0) \approx 0.5$. The experimentally observed rise of the cross sections at high energy has lead Pomeranchuk to propose the existence of a pole with $\alpha(0) \gtrsim 1$ which corresponds to the exchange of objects with vacuum quantum numbers. The corresponding quasi-particle is called the pomeron. Its trajectory should be related to glueballs instead of mesons or baryons. So far the existence of glueballs could not be confirmed experimentally.

Another problem of Eq. (7) is the violation of unitarity at high energy. This is most obvious by noting that the elastic cross section is predicted to finally exceed the total one or that the Froissart-Martin bound $\sigma^{\text{tot}} < c \ln^2 s$ is violated.

Despite of these shortcomings, Regge pole motivated parametrizations are rather successful in predicting high-energy cross sections in the currently accessible energy range ^{10,11}. For example, Fig. 3a shows the prediction by

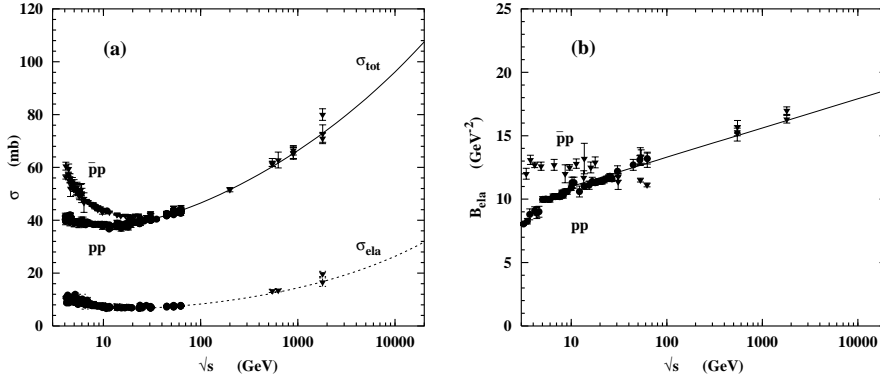


Figure 3. Comparison of a simple Regge fit using two poles with pp and $p\bar{p}$ data. The parameters for the total cross section fit are from ¹⁰.

Donnachie and Landshoff ¹⁰ together with pp and $p\bar{p}$ data. In Fig. 3b we

show the energy dependence of the elastic slope parameter, B_{ela} , which is also in agreement with the simple Regge pole expectation of a logarithmic energy dependence (see Eq. (10)).

3.2 Multi-pomeron models

As already mentioned, the pomeron exchange amplitude violates unitarity. Although this doesn't seem to be a serious problem at current collider energies, it indicates an inconsistency of this model.

The simplest way of overcoming this problem without abandoning Regge theory altogether is the introduction of multiple pomeron exchanges in a single scattering process. Assuming that large momentum transfers are suppressed by the dynamics of the strong interaction, as it is the case in QCD, multi-pomeron exchange can be described on the basis of Gribov's Reggeon field theory (RFT) ¹². Then the total amplitude can be written as the sum of n -pomeron exchange amplitudes $A^{(n)}(s, t)$. For each n -pomeron graph one can define a theoretical "total" cross section applying the optical theorem to the corresponding n -pomeron amplitude

$$\sigma^{(n)} = (-1)^{n+1} \frac{1}{s} \Im m \left(A^{(n)} \right), \quad \sigma_{\text{tot}} = \sum_{n=1}^{\infty} (-1)^{n+1} \sigma^{(n)}. \quad (11)$$

Here the alternating sign has been introduced by definition to keep all partial cross sections $\sigma^{(n)}$ positive.

As a simplified model we consider only the first two graphs shown in Fig. 4, assuming $\sigma^{(n)} \ll 4\sigma^{(2)} < \sigma^{(1)}$ with $n > 2$. Then, the total cross section reads

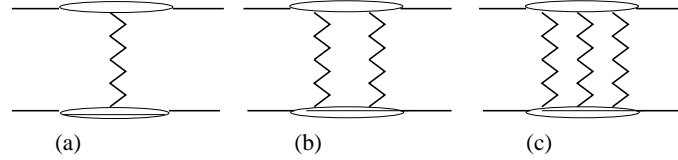


Figure 4. Hadron-hadron scattering via pomeron exchange: (a) one-pomeron, (b) two-pomeron, and (c) three-pomeron exchange graphs.

$\sigma_{\text{tot}} = \sigma^{(1)} - \sigma^{(2)}$, where $\sigma^{(1)}$ and $\sigma^{(2)}$ are the cross sections of the one- and two-pomeron exchange graphs, respectively. The energy-dependence of the two-pomeron cross section is directly linked to that of $\sigma^{(1)} \sim s^{\Delta}$ and turns out to be $\sigma^{(2)} \sim s^{2\Delta}$. The two-pomeron cross section grows faster with energy than the one-pomeron cross section. This leads to a weaker energy-dependence of the total cross section than in the single-pomeron exchange model.

One particular realization of the multi-pomeron exchange is the eikonal model using the pomeron amplitude as eikonal function. In general, predictions of such models are in good agreement with cross section data and are nearly indistinguishable from the single-pomeron exchange model in the energy range up to several TeV c.m.s. energy.

3.3 Photon-induced hadronic interactions

The generalization to photon-induced interactions is straight-forward in terms of the generalized vector dominance model (GVDM) ^{13,14}. The photon is considered as a superposition of two types of states, a bare photon and hadronic fluctuations. With the probability of the order of the fine structure constant α_{em} the photon can be found in a fluctuation which interacts like a hadron. Since the cross section of the bare photon is small it can be neglected in most applications. In the proton rest frame, the life time t_f of the hadronic fluctuation with momentum k and mass M is much larger than the typical interaction time t_i

$$t_f \sim \frac{1}{\sqrt{M^2 + k^2} - \sqrt{-Q^2 + k^2}} \approx \frac{2k}{M^2 + Q^2} , \quad (12)$$

where Q^2 denotes the photon virtuality. The hadronic amplitudes for the scattering of longitudinally (L) and transversely (T) polarized photons are written as

$$A_{\gamma h \rightarrow X}^{(T)} = \sum_V \left(\frac{e}{f_V} \right) \frac{m_V^2}{m_V^2 - q^2 - i\Gamma_V m_V} A_{Vh \rightarrow X}^{(T)}(s, t) \quad (13)$$

$$A_{\gamma h \rightarrow X}^{(L)} = \sum_V \left(\frac{e}{f_V} \right) \left(\frac{-q^2 \xi_V}{m_V^2} \right)^{\frac{1}{2}} \frac{m_V^2}{m_V^2 - q^2 - i\Gamma_V m_V} A_{Vh \rightarrow X}^{(T)}(s, t) , \quad (14)$$

with q , m_V , and Γ_V being the four-momentum of the incoming photon and the mass and the decay width of the vector meson V , respectively. $A_{Vh \rightarrow X}^{(T)}$ is the amplitude for the scattering of the transversely polarized vector meson V off the hadron h . The parameter ξ_V is introduced to allow for different cross sections of transversely and longitudinally polarized vector mesons.

The GVDM is very successful in predicting the total and quasi-elastic vector meson photoproduction cross sections ¹⁵. However, the s -dependence of the γp and $\gamma\gamma$ cross sections changes considerably from real to virtual photons. This cannot be understood on the basis of GVDM alone. Many alternative models have been published. The most promising calculations combine within the color-dipole framework ideas of GVDM with perturbative QCD calculations, obtaining a reasonable description of the measurements ¹⁶.

3.4 Impact parameter picture of high-energy scattering

The impact parameter picture of high-energy scattering is very useful for discussing effects related to the wave character of the scattering particles. Its meaning becomes most transparent by considering again the partial wave expansion of the scattering amplitude

$$A(s, t) = 16\pi \sum_{l=0}^{\infty} (2l+1) a_l(s) P_l(\cos \theta). \quad (15)$$

In the classical (geometrical) description, the l th term on the r.h.s. of Eq. (15) with angular momentum l is assumed to correspond to the interaction of two particles with an impact parameter \vec{b} satisfying $l = |\vec{b}|k$. The impact parameter vector \vec{b} is by definition perpendicular to the momentum \vec{k} of the incoming particle. At high energy the sum can be approximated by the integral

$$A(s, t) = 16\pi \int_0^{\infty} dl (2l+1) a_l(s) P_l(\cos \theta), \quad (16)$$

using for $a_l(s)$ the analytic continuation in l . Taking the limit $P_l(\cos \theta) \xrightarrow{l \rightarrow \infty} J_0[(2l+1)\sin(\theta/2)]$ and substituting

$$J_0(z) = \frac{1}{2\pi} \int_0^{2\pi} d\varphi e^{iz \cos \varphi}, \quad \vec{b} \cdot \vec{q} = \vec{b} \cdot \vec{q}_{\perp} = b q_{\perp} \cos \varphi, \quad (17)$$

Eq. (16) becomes

$$A(s, t) = 4s \int d^2\vec{b} a(s, \vec{b}) e^{i\vec{q}_{\perp} \cdot \vec{b}}, \quad \text{with} \quad a(s, \vec{b}) = a_l(s) \big|_{l=kB}. \quad (18)$$

The impact parameter amplitude $a(s, \vec{b})$ is the Fourier transform of the elastic scattering amplitude. Furthermore, in analogy to geometrical optics, the function $a(s, \vec{b})$ can be interpreted as the density function of sources of scattered waves producing interference patterns. The total and elastic cross sections are given by

$$\sigma_{\text{ela}}(s) = 4 \int d^2\vec{b} |a(s, \vec{b})|^2, \quad \sigma_{\text{tot}}(s) = 4 \int d^2\vec{b} \Im m(a(s, \vec{b})). \quad (19)$$

For an amplitude with exponential t -dependence $A(s, t) \sim i s \sigma_{\text{tot}} \exp\{\frac{1}{2} B_{\text{ela}} t\}$ the corresponding impact parameter amplitude reads

$$a(s, \vec{b}) = i \frac{\sigma_{\text{tot}}}{8\pi B_{\text{ela}}} \exp\left(-\frac{\vec{b}^2}{2B_{\text{ela}}}\right). \quad (20)$$

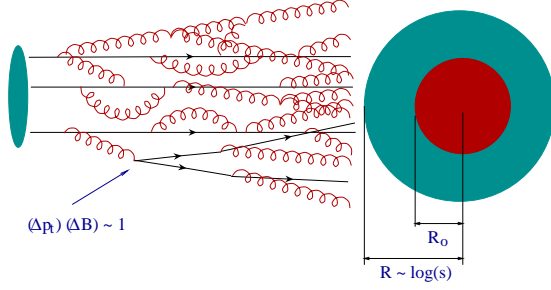


Figure 5. Partonic interpretation of the logarithmic growth of hadrons with energy.

The width of the amplitude in \vec{b} -space (i.e. the “gray” area) is given by the t -slope of the elastic cross section and, according to Eq. (10), grows logarithmically with s . This can also be understood in terms of partons in a hadron as shown in Fig. 5. Each parton splitting involves a transverse momentum transfer which corresponds to a small displacement in impact parameter. The total displacement of a parton follows from the number of steps N of its random walk, $R^2 \sim \Delta b \cdot N \sim (\Delta p_\perp)^{-1} \ln s$. This picture also readily explains why the elastic slope of hard processes has a much weaker energy dependence: the displacement in \vec{b} is much smaller because of the larger Δp_\perp .

From the unitarity constraint $|a(s, \vec{b})| < 1$ one gets as high-energy limit $\sigma_{\text{tot}} < c \ln^2 s$ with c being a constant. The special case of the black disk limit (e.g. maximum absorption) corresponds to $a(s, \vec{b}) = i/2$ for $b < R$ and $a(s, \vec{b}) = 0$ otherwise. Then the inelastic cross section (cross section for absorption) is given by the geometrical size of the disk $\sigma_{\text{ine}} = \pi R^2$ whereas the total cross section is twice the disk size, $\sigma_{\text{tot}} = 2\pi R^2$. This is a result of unitarity: absorption gives rise to elastic scattering $\sigma_{\text{ela}} = \pi R^2 = \sigma_{\text{tot}}/2$.

4 Multiparticle production

4.1 Unitarity and cuts

To link particle production to elastic scattering amplitudes one can use the optical theorem. In terms of Feynman diagrams a particle propagator collapses to an external on-shell particle line if its imaginary part is taken

$$\Im m \left(\frac{1}{p^2 - m^2 - i\epsilon} \right) = \pi \delta(p^2 - m^2) . \quad (21)$$

Therefore taking the discontinuity (i.e. the imaginary part) of a propagator is commonly referred to as “cutting”. This is also the reason why, up to kin-

matical factors, the discontinuity of elastic amplitude is equal to the squared matrix element describing particle production, as sketched in Fig. 6.

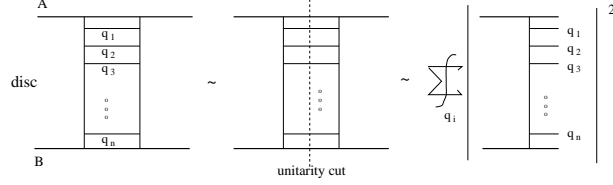


Figure 6. Graphical representation of optical theorem.

One particular application is the discussion of the topologies of cut pomeron and reggeon amplitudes in the limit of large numbers of colors and flavours in QCD¹⁷. As depicted in Fig. 7 the dominant final state contributions are a two- and one-string configurations.

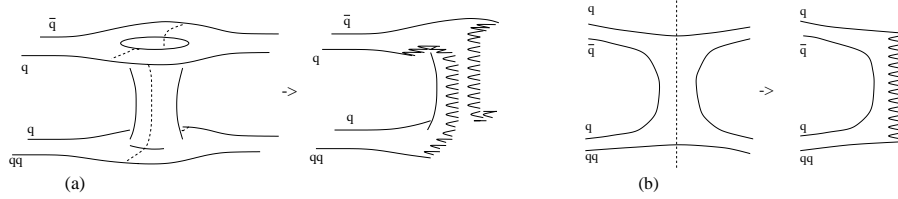


Figure 7. Cuts and final state topologies of (a) pomeron and (b) reggeon exchange graphs.

4.2 Abramovski-Gribov-Kancheli cutting rules

In general, there are many possibilities of cutting diagrams involving multiple pomerons. The dominant contribution of the different cut configurations to the total discontinuity can be calculated with the Abramovski-Gribov-Kancheli (AGK) cutting rules¹⁸:

- (i) The dominant contributions are given by cut configurations where the cut involves all intermediate particle states of a pomeron (a contribution due to a partially cut pomeron is sub-leading).
- (ii) For an n -pomeron exchange graph, the contribution to the discontinuity with ν cut pomeron propagators is $B_\nu^n 2\Im m(A^{(n)})$. Here, $A^{(n)}$ denotes the n -pomeron amplitude and ν is restricted to $0 \leq \nu \leq n$. The combinatorial

factors (AGK weights) B_ν^n are

$$B_\nu^n = \begin{cases} (-1)^{\nu-1} \frac{n!}{\nu!(n-\nu)!} 2^{n-1} : \nu \geq 1 \\ 1 - 2^{n-1} : \nu = 0 . \end{cases} \quad (22)$$

(iii) The coefficients B_ν^n satisfy $\sum_{\nu=0}^n B_\nu^n = 1$, which means that all leading contributions to the total discontinuity are included.

For example, there are three leading cuts of the two-pomeron graph (Fig. 4b): the diffractive cut with the weight -1 (Fig. 8a), the one-pomeron cut with the weight 4 (Fig. 8b), and the two-pomeron cut with the weight -2 (Fig. 8c). The cross sections for the different final states of the two-pomeron

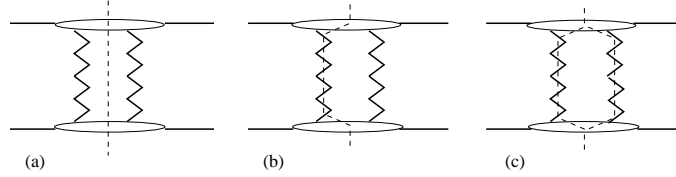


Figure 8. Breakdown of the total discontinuity of the two-pomeron exchange graph according to the AGK cutting rules: (a) the diffractive cut describing low-mass diffraction, (b) the one-pomeron cut, and (c) the two-pomeron cut.

exchange graph are (a) diffractive cut: $\sigma_{\text{diff}} = \sigma^{(2)}$, (b) one-pomeron cut: $\sigma_1 = -4\sigma^{(2)}$, and (c) two-pomeron cut: $\sigma_2 = 2\sigma^{(2)}$, see Fig. 9. Note that the diffractive cut of the two-pomeron graph gets a negative AGK weight, hence giving in total a positive, experimentally observable cross section. However, the cross section for the one-pomeron cut of the two-pomeron graph is negative. Since the one-pomeron cut of the one-pomeron graph has the same inelastic final state as the one-pomeron cut of the two-pomeron graph (Fig. 9b), one can sum both contributions to obtain a positive cross section.

Let's consider again the example of the one- and two-pomeron graphs. Concerning the topologies of the final state particles, the total cross section is built up of the sum of the partial cross sections of the one- and two-pomeron exchange graphs: (i) one-pomeron cut $\sigma_1 = \sigma^{(1)} - 4\sigma^{(2)}$, (ii) two-pomeron cut $\sigma_2 = 2\sigma^{(2)}$, and (iii) diffractive cut of the two-pomeron graph $\sigma_{\text{diff}} = \sigma^{(2)}$.

The particle density in pseudorapidity due to a one-pomeron cut is assumed to be almost energy independent (which is true for longitudinal phase space models) and is denoted by $dN_1/d\eta$. Provided the two-pomeron cut gives two times the particle yield as compared to the one-pomeron cut (in central

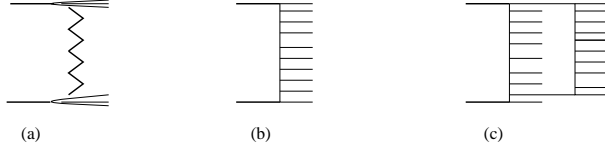


Figure 9. Inelastic final states resulting from (a) the diffractive cut describing low-mass diffraction, (b) the one-pomeron cut, and (c) the two-pomeron cut.

pseudorapidity region, see Fig. 9), the inclusive inelastic charged particle cross section is given by

$$\left. \frac{d\sigma_{\text{ch}}}{d\eta} \right|_{\eta \approx 0} = 1 \times \sigma_1 \frac{dN_1}{d\eta} + 2 \times \sigma_2 \frac{dN_1}{d\eta} + 0 \times \sigma_{\text{diff}} \frac{dN_1}{d\eta} = \sigma^{(1)} \frac{dN_1}{d\eta}. \quad (23)$$

Due to the topology of diffractive final states, almost no particles are produced in the central region in the case of a diffractive cut. Note that only the one-pomeron graph determines the inclusive particle cross section in the central region (AGK cancellation).

On the other hand, the inclusive charged particle density follows from

$$\left. \frac{dn_{\text{ch}}}{d\eta} \right|_{\eta \approx 0} = \frac{\sigma^{(1)}}{\sigma_{\text{tot}}} \left. \frac{dN_1}{d\eta} \right|_{\eta \approx 0} \approx \frac{\sigma^{(1)}}{\sigma^{(1)} - \sigma^{(2)}} \left. \frac{dN_1}{d\eta} \right|_{\eta \approx 0}. \quad (24)$$

Eq. (24) allows us to understand the observed behaviour of $\rho(0) = dn_{\text{ch}}/d\eta$ in pp and $p\bar{p}$ collisions. With $\sigma^{(1)} \sim s^\Delta$ and $\sigma_{\text{tot}} \sim s^{0.08}$, one gets a power-law increase of the central particle density. This is confirmed by experiment¹⁹: $\rho(0) \approx 0.74 s^{0.105}$.

Since the two-pomeron graph has a cross section which increases faster with energy than the cross section of one-pomeron graph, the model predicts also an increase of the multiplicity fluctuations with increasing collision energy. In a model without geometric scaling this leads to violation of KNO scaling²⁰ at high energies. Furthermore, due to the characteristic structure of the one- and two-pomeron cuts, strong long-range correlations in pseudorapidity are naturally explained. For a detailed discussion, see for example⁵ and Refs. therein.

Finally, as a representative example, model predictions for the multiplicity distribution and the pseudorapidity distribution (calculated with the PHOJET event generator²¹) are compared with collider data¹⁹ in Fig. 10.

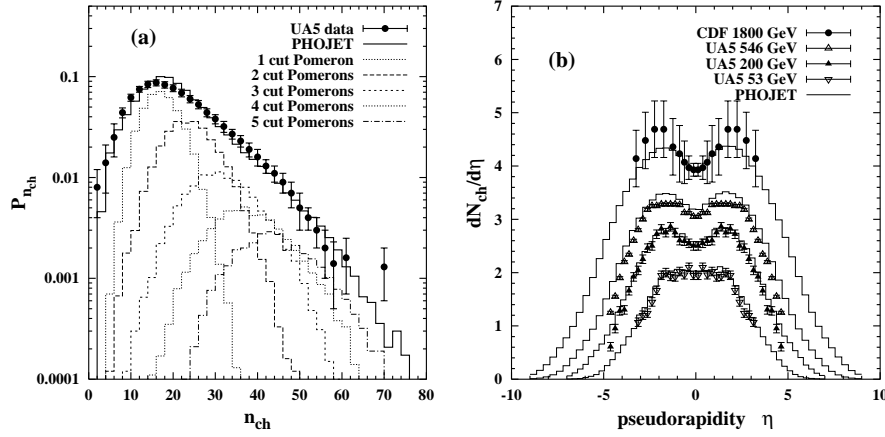


Figure 10. (a) Decomposition of the multiplicity distribution in $p\bar{p}$ collisions according to the number of generated pomeron cuts at $\sqrt{s} = 200$ GeV. (b) Energy-dependence of charged particle pseudorapidity density in $p\bar{p}$ collisions.

5 Summary

Regge theory, AGK cutting rules, QCD in the limit of large numbers of colors and flavours, and the geometrical interpretation of high-energy scattering prove very useful in understanding the basic properties of cross sections and multiparticle production. They are some of the tools available today to study soft processes theoretically. Many models combine them to obtain a detailed description of soft processes^{5,22,23,21,24}.

However we are far from being able to reliably calculate predictions for most soft production processes. All approaches or models discussed here have severe shortcomings. For example, Regge theory does not predict transverse momentum-related quantities, and most models implement AGK cutting rules without energy-momentum conservation, to name but a few. Furthermore the rather large number of free parameters limits the predictive power of calculations.

Acknowledgements: This work is supported by U.S. Department of Energy grant DE-FG02 91ER 40626. The author is grateful to L. Frankfurt, T.K. Gaisser, J. Ranft, S. Roesler, T. Stanev, and M. Strikman for many interesting discussions.

References

1. C. T. Sachrajda: Phenomenology from lattice QCD, (hep-ph/0110304), 2001
2. V. A. Khoze and W. Ochs: Theory of multiparticle production in the soft region, MPI-PHT-2001-42 (hep-ph/0110295), 2001
3. A. B. Kaidalov: Phys. Rep. 50 (1979) 157
4. P. D. B. Collins and A. D. Martin: Rep. Prog. Phys. 45 (1982) 335
5. A. Capella, U. Sukhatme, C. I. Tan and J. Trần Thanh Vân: Phys. Rep. 236 (1994) 225
6. H. Abramowicz, L. Frankfurt and M. Strikman: Surveys High Energ. Phys. 11 (1997) 51
7. E. Levin: An introduction to pomerons, (hep-ph/9808486), 1998
8. A. B. Kaidalov: Surveys High Energ. Phys. 13 (1999) 265
9. P. D. B. Collins: *An Introduction to Regge Theorie & High Energy Physics*, Cambridge University Press, Cambridge 1977
10. A. Donnachie and P. V. Landshoff: Phys. Lett. B296 (1992) 227
11. Particle Data Group: D. E. Groom et al.: Eur. Phys. J. C15 (2000) 1
12. V. N. Gribov: Sov. Phys. JETP 26 (1968) 414; M. Baker and K. A. Ter-Martirosyan: Phys. Rep. 28C (1976) 1
13. J. J. Sakurai and D. Schildknecht: Phys. Lett. 41B (1972) 489
14. T. H. Bauer, R. D. Spital, D. R. Yennie and F. M. Pipkin: Rev. Mod. Phys. 50 (1978) 261; erratum Rev. Mod. Phys. 51 (1979) 407
15. H. Abramowicz and A. Caldwell: Rev. Mod. Phys. 71 (1999) 1275
16. B. Badelek and J. Kwieciński: Phys. Lett. B295 (1992) 263; A. D. Martin, M. G. Ryskin and A. M. Stasto: Eur. Phys. J. C7 (1999) 643; E. Gotsman, E. Levin, U. Maor and E. Naftali: Eur. Phys. J. C10 (1999) 689; M. McDermott, L. Frankfurt, V. Guzey and M. Strikman: Eur. Phys. J. C16 (2000) 641
17. G. Veneziano: Nucl. Phys. B117 (1976) 519
18. V. A. Abramovski, V. N. Gribov and O. V. Kancheli: Sov. J. Nucl. Phys. 18 (1974) 308
19. C. Geich-Gimbel: Int. J. Mod. Phys. A4 (1989) 1527
20. Z. Koba, H. B. Nielsen and P. Olesen: Nucl. Phys. B40 (1972) 317
21. R. Engel and J. Ranft: Phys. Rev. D54 (1996) 4244
22. A. B. Kaidalov and O. I. Piskunova: Z. Phys. C30 (1986) 145
23. P. Aurenche *et al.*: Phys. Rev. D45 (1992) 92; S. Roesler, R. Engel and J. Ranft: The Monte Carlo event generator DPMJET-III (hep-ph/0012252)
24. H. J. Drescher, M. Hladik, S. Ostapchenko, T. Pierog and K. Werner: Phys. Rep. 350 (2001) 93